Soft Matter

PAPER

Effects of Chemically Heterogeneous Nanoparticles on Polymer Dynamics: Insights from Molecular Dynamics Simulations

Received 00th January 20xx,
Accepted 00th January 20xx

DOI: 10.1039/x0xx00000x

www.rsc.org/

Zijian Zheng,[ab] Fanzhu Li,[a] Jun Liu,[*a] Raffaele Pastore,[c,d] Guido Raos,[d] Youping Wu,[a] Liqun Zhang [*a]

The dispersion of solid nanoparticles within polymeric materials is widely used to enhance their performance. Many scientific and technological aspects of the resulting polymer nanocomposites have been studied, but the role of the structural and chemical heterogeneity of nanoparticles has just started to be appreciated. For example, simulations of polymer films on planar heterogeneous surfaces revealed unexpected, non-monotonic activation energy to diffusion on varying the surface composition. Motivated by these intriguing results, here we simulate via molecular dynamics a different, fully three-dimensional system, in which heterogeneous nanoparticles are incorporated in a polymer melt. The nanoparticles are roughly spherical assemblies of strongly and weakly attractive sites, in fraction *f* and 1-*f*, respectively. We show that polymer diffusion is still characterized by non-monotonic dependence of the activation energy on *f*. The comparison with the case of homogeneous nanoparticles clarifies that the effect of the heterogeneity increases on approaching the polymer glass transition.

I. Introduction

The introduction of nanoparticles (NPs) into polymer matrices is an effective strategy to fabricate high performance polymer nanocomposites (PNCs)[1-3]. A fundamental understanding of their composition-structure-properties relationship will facilitate the further development of materials with desired properties[4]. One key lesson is that it is crucial to disperse the nanoparticles well in the polymer matrix in order to produce high performance composites[5]. This can be achieved by compatibilizing them, for example by coating the nanoparticles or grafting them with the polymer[6-8].

The interface between polymers and nanoparticles is also a very important element. In the nanometer-size interstices between the nanoparticles, the polymer chains become severely restricted and may deviate substantially from their bulk behavior[9]. Thus, the polymer interfaces which are formed near solid surfaces and nanoparticles have received wide consideration from both the academic and industrial communities[10-14]. One of the earliest studies is the one by

[a] *Key Laboratory of Beijing City on Preparation and Processing of Novel Polymer Materials, State Key Laboratory of Organic-Inorganic Composites, Beijing University of Chemical Technology, 100029 Beijing, China*
E-mail: liujun@mail.buct.edu.cn, zhanglq@mail.buct.edu.cn.
[b] *Hubei Collaborative Innovation Center for Advanced Organic Chemical Materials, Key Laboratory for the Green Preparation and Application of Functional Materials, Ministry of Education, Hubei Key Laboratory of Polymer Materials, School of Materials Science and Engineering, Hubei University, 430062 Wuhan, China*
[c] *CNR-SPIN, Via Cintia, 80126 Napoli, Italy*
[d] *Dipartimento di Chimica, Materiali e Ingegneria Chimica "G. Natta", Politecnico di Milano, via L. Mancinelli 7, 20131 Milano, Italy*

Tsagaropoulos and Eisenberg[15], who observed that several polymer properties such as viscosity, diffusion coefficient, and the T_2 relaxation time in NMR measurements were drastically altered by silica nanoparticles and attributed this effect to a drastic slowing down of the chains in the interfacial region. Later on, Torkelson and coworkers[16, 17] studied the relaxation of thin polymer films on silica surfaces, as a model for polymer-silica nanocomposites. Using fluorescent probes to monitor the dynamics of the polymer matrix, they demonstrated that chains next to the surface were nearly completely arrested (at temperatures above the bulk T_g), but the slowing down in the relaxation dynamics could be felt up to 100 nm away from it. Even a small concentration of nanoparticles can slow down significantly the polymer diffusion within a PNC, due to a combination of the reduced polymer relaxation and the entropic barriers created by the excluded volume of the NPs[18]. NP induced enhancement of the polymer relaxation rate has been also observed for particular physical situations, including systems formed by entangled polymers and NPs smaller than the entanglement mesh size[19].

Many useful insights have been obtained by theoretical analyses and molecular dynamics (MD) or Monte Carlo simulations, alongside the traditional experimental methods[20-22]. Smith et al.[23] introduced some structural roughness in the coarse-grained modelling of NPs. Starr et al.[24] found a mobility gradient for coarse-grained polymer chains approaching the nanoparticle surfaces, both for repulsive and attractive polymer/nanoparticle interactions. Li et al.[25] explored the dynamics of long polymer chains filled with spherical NPs. Through a primitive path analysis, they showed that the chains become significantly disentangled on increasing the NP volume fraction, but "NP entanglements" become significant above a critical volume fraction. More recently, Hagita et al.[26] have performed large-scale MD simulations of related cross-linked models, to describe the mechanical deformation of rubbery nanocomposites with different degrees of particle aggregation. At the atomistic level of description, Ndoro et al.[27] simulated a composite consisting of ungrafted and grafted spherical silica nanoparticles embedded in a melt of 20-monomer atactic polystyrene chains. These showed that the nanoparticles modify the polymer structure in its neighborhood, and these changes increase with the higher grafting densities and larger particle diameters. De Nicola et al.[28] used the results of molecular simulation as a guide for the preparation of improved polymer-NP composites, exploiting an *in situ* polymerization of macromonomers.

Most of the previous simulations, especially those based on coarse-grained models, employed completely smooth or structured NPs with chemically uniform surfaces. However the most common fillers, namely silica[29] and especially carbon black[30, 31] for applications involving mechanical reinforcement, have heterogeneous surfaces exposing a range of functional groups and adsorption sites (e.g., both hydrophobic and hydrophilic, hydrogen-bonding groups). Note that the slight roughness of an atomically structured surface has already a very significant effect on the polymer dynamics, in comparison to the idealized situation with a perfectly smooth surface[32]. An even greater effect can be expected from the introduction of some chemical heterogeneity in the surfaces and/or the polymer. In fact, there is ample evidence that this sort of ''quenched'' disorder plays an important role in many aspects of polymer behavior[33]. Recent insights came from MD simulations of thin polymer films adsorbed on structurally and chemically heterogeneous surfaces. These latter are composed by randomly assembling on a planar square lattice two type of beads, strongly (S) and weakly (W) attractive, in variable percentage. In such a quasi-2D model, the dynamic slowdown of polymers was found to depend non-monotonically on the surface composition: the activation energy to diffusion and the inverse glass transition temperature do not attain a maximum for 100% of strong sites, but at a smaller value, about 75%, which originates as a compromise between the maximum global attraction and the maximum configurational disorder at the random percolation (50%) of strong sites. In addition, new dynamical features, which are not observed on a smooth surface, become more and more apparent on increasing the

surface heterogeneity. These include temporary subdiffusive regimes followed by "Fickian yet not Gaussian diffusion" as well as stretched exponential relaxation of the Rouse Normal Modes autocorrelation functions.

In this paper, we aim at understanding whether these intriguing benchmarks are also relevant to fully three-dimensional polymer nanocomposite, where NPs are finely dispersed within the polymer melts. This is not a trivial question, since the different dimensionality, the coexistence of adsorbed and non-adsorbed polymers as well as the presence of NP induced steric interactions make this physical situation markedly distinct from that described in Ref.s[34,35]. We investigate this issue by introducing a coarse-grained model of polymer melt embedding a number of heterogeneous NPs. Each NP consists in a roughly spherical assembly of W and S sites. Performing extensive MD simulations, we investigate the polymer dynamics at different temperatures and variable NP composition. We find that, in spite of the difference between the two physical situations, some dynamical signatures found in Refs.[34,35] survive in this system, suggesting the existence of a common underlying physical mechanism. In addition, we clarify to what extent the heterogeneous nature of the NPs modifies the polymer dynamics compared to the homogeneous case, showing that relatively small differences at high temperature may result in dramatic change close the polymer glass transition.

II. Simulation model and method

In our coarse-grained model, the heterogeneous NPs are roughly spherical and are composed by two types of randomly distributed beads, which may be either of the weak (W) or the strong (S) type, the only difference being the interaction energy with polymers. A snapshot is shown in Fig. 1. Briefly, we first generate one NP, formed by N=128 beads, N_e=74 of which are exposed, and replicate such a prototype within the simulation box until the desired number of NPs is reached. At this stage, we randomly assign the interaction energy (i. e. the type) to each bead with probability f and 1-f for strong (S) and weak (W) interactions, respectively.[36]

The simulation box contains 30 nanoparticles, which corresponds to a volume fraction of NPs φ=0.253 (estimated from the total numbers of NP-type and polymer-type beads). During the MD simulations, the NPs are modelled as perfectly rigid bodies, with only three translational and three rotational degrees of freedom.

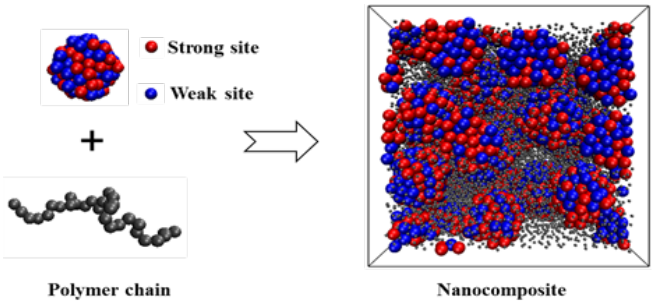

Fig. 1 The snapshots of nanoparticle, polymer chain and the corresponding nanocomposite. Within the NPs, the blue spheres represent the S sites and the red spheres represent the W sites.

The polymer chains are fully flexible and are represented by a generic bead-spring model. Overall, each polymer chain contains 32 beads. Given the relatively short length of the polymer chains, entanglement effects play a minor role on the system dynamics. Roughly, each bond of the coarse-grained model would correspond to 3-6 covalent bonds along the backbone of a chemically realistic chain. However, since we are not interested in a specific polymer, it is unnecessary to attempt a precise mapping. We adopt a "reduced" set of units, whereby the mass m and diameter σ of each bead-which are identical for the polymer and the NPs-are effectively equal to unity. The non-bonded interactions between all the beads are modeled by truncated and shifted Lennard-Jones (LJ) potentials:

$$U(r) = \begin{cases} 4\varepsilon\left[\left(\frac{\sigma}{r}\right)^{12} - \left(\frac{\sigma}{r}\right)^{6}\right] + C & r < r_{cutoff} \\ 0 & r \geq r_{cutoff} \end{cases} \quad (1)$$

where C is a constant which guarantees that the potential energy is continuous at $r=r_{cutoff}$, and ε is the energy scale of the

model. While the effective diameter σ is the same for all beads, both the interaction energy and the cutoff distance depend on the combination of bead types. The interaction strength between the polymer beads (P) and the S sites is twice that of the other pairs. Thus $\varepsilon_{PP}=\varepsilon_{PW}=\varepsilon$ and $\varepsilon_{PS}=2\varepsilon$. All the polymer-NP interactions are truncated at a cutoff distance of $r_{PW}=r_{PS}=2.5\sigma$, whereas the polymer–polymer interactions are truncated at $r_{PP}=2^{1/6}\sigma$ to produce a purely repulsive potential. Also the interaction between the beads belonging to different NP is modelled with $\varepsilon_{NN}=\varepsilon$ (where N=W or S) and the cutoff $r_{NN}=2^{1/6}\sigma$, so as to promote their dispersion within the polymer matrix. By doing so, we aim at modelling the physical situation of finely dispersed NPs within the polymer melts, which can be achieved in different experimental setups, such as samples freshly rejuvenated at high shear rate. In systems of this kind, the typical separation distance between NPs is large enough to make van der Waals interactions negligible.

The interaction between bonded beads within a polymer is modeled by adding a finite extensible nonlinear elastic (FENE) potential to their LJ interaction:

$$U_{FENE} = -0.5kR_0{}^2 ln\left[1-\left(\frac{r}{R_0}\right)^2\right] \qquad (2)$$

where $k=30\varepsilon/\sigma^2$ is the force constant and $R_0=1.3\sigma$ is the maximum extensibility of the bonds. The finite extensibility of the bonds avoids chain crossing events without introducing high-frequency bond vibrations, which would be produced by very stiff harmonic bonds. The relatively short maximum bond length enhances the polymer's resistance to ordering and crystallization, by increasing the mismatch between bonded and non-bonded nearest-neighbor distances (the actual equilibrium bond length, resulting from the balance between LJ and FENE interactions, is about 0.8σ)[37]. The reduced number density of the monomer was fixed at $\rho^*=1.00$, which corresponds to that of a dense melt. This is also roughly equal to the density inside the NPs. Units are reduced so that $\sigma=m=\varepsilon=k_B=1$, where k_B is the Boltzmann's constant.

We have performed NVT molecular dynamics simulations, using a Nose-Hoover thermostat and velocity-Verlet algorithm to integrate the equations of motion. Periodic boundary conditions are applied to all three directions. The average MD run consists of 10^9 time steps. All the simulations have been carried out with a large scale atomic/molecular massively parallel simulator (LAMMPS), developed by the Sandia National Laboratories[38]. Further simulation details can be found in our previous work[39,40].

III. Results

3.1 Translational dynamics

We start by investigating the effect of heterogeneous NPs on the translational dynamics of the whole polymer chains. To this aim, Fig. 2 shows the time dependence of the mean square displacements (MSDs) of the polymer center of mass, for different NP composition, *f*, and temperature, T^*. The mobility of the polymer chains becomes small on lowering the temperature and for large values of f and display an increasingly long lasting subdiffusive behaviuour. However, even for the slowest system, the diffusive regime is restored within the timescale of our simulations,

$$\langle\left(r_{cm}(t)-r_{cm}(0)\right)^2\rangle = 6\,D\,t \qquad (3)$$

allowing to estimate the chain diffusion coefficient, *D*, a long time fit to the MSD data. The diffusion coefficient so measured are listed in Table 1 and plotted in Fig. 3a shows as a function of temperature and at different values of f. This figure clarifies that the data can be properly fitted using an Arrhenius functional law:

$$ln(D) = ln(D_0) - E_a/T^* . \qquad (4)$$

The values of the activation energies (E_a) obtained from these fits are plotted in Figure 3b as a function of the NP composition, f, and listed in the last line of Table 1.

Table 1. Polymer Diffusion Coefficients for Each Reduced Temperature (T^*) and Surface Composition (f).The last row gives the activation energies at different Surface Composition (f).

T^*/f	Neat	0.00	0.25	0.50	0.75	1.00
0.7	0.0019	4.84×10^{-5}	2.98×10^{-5}	1.62×10^{-5}	1.22×10^{-5}	1.15×10^{-5}
0.8	0.0021	7.63×10^{-5}	4.25×10^{-5}	3.54×10^{-5}	2.23×10^{-5}	1.93×10^{-5}
0.9	0.0023	1.11×10^{-4}	6.99×10^{-5}	4.89×10^{-5}	3.91×10^{-5}	2.94×10^{-5}
1.0	0.0026	1.48×10^{-4}	1.05×10^{-4}	7.31×10^{-5}	5.66×10^{-5}	4.37×10^{-5}
1.1	0.0027	1.88×10^{-4}	1.26×10^{-4}	1.02×10^{-4}	8.06×10^{-5}	6.41×10^{-5}
1.2	0.0030	2.08×10^{-4}	1.65×10^{-4}	1.32×10^{-4}	1.08×10^{-4}	8.95×10^{-5}
E_a	0.71±0.01	2.52±0.05	2.96±0.03	3.43±0.02	3.67±0.03	3.42±0.02

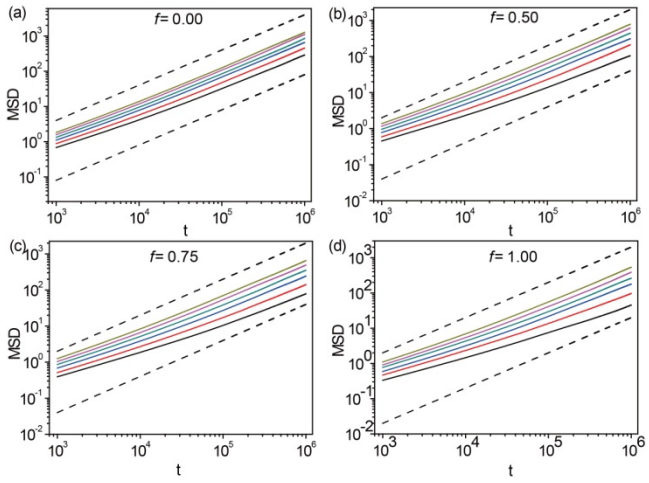

Fig. 2 Mean square displacement as a function of time, for T^* = 1.2, 1.1, 1.0, 0.9, 0.8, and 0.7 from top to bottom. Different panels report different values of f, as indicated. Dashed lines are guides to the eye of slope 1.

Overall, the order of magnitude of the activation energy is compatible with the results of previous work investigating different polymer nanocomposite systems[35]. For the neat polymer system, E_a is due to crowding and excluded volume effect, and therefore has an entropic origin. The presence of NPs introduces attractive interaction and increases the crowding effect. This results in significantly higher activation energy, even for f=0. In addition Fig. 3(b) shows that E_a as a function f in Fig. 3(b) is maximal around f=0.75. This non-monotonic behaviour is intriguing, as the largest activation energy to diffusion does not correspond to the situation where the strength of the interaction is overall the largest, f=1, but to a lower value of f. As previously mentioned, a similar result emerged from the simulations of polymer films adsorbed on heterogeneous planar surfaces of Ref.s[34,35]. In that case, the value f=0.75 was interpreted as the compromise between the largest overall interaction energy (f=1) and the maximum structural disorder, attained at the random percolation transition of strong sites (occurring around f=0.5, in two dimensions). This scenario was validated by an analysis of the surface induced energy landscape, as probed by horizontally sliding a single bead along the surface at very low temperature. The average value of the energy barriers linearly increases between *f=0* and *f=1*, whereas the standard deviation is the largest for the most disordered substrate *f=0.5*. Finally, the most

significant descriptor of the dynamics are the tails of energy barrier distributions that are indeed the largest at *f=0.75*. Considering the similar behaviour found in the present model, we speculate that the shape of the energy landscape and its implications are also similar.

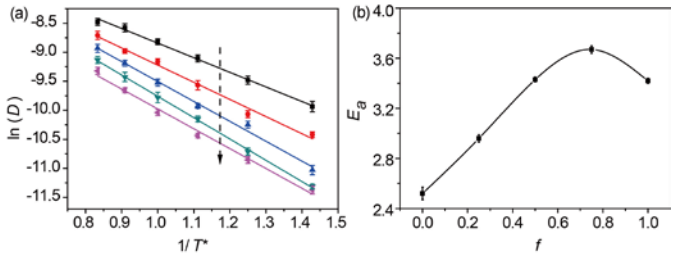

Fig. 3 Arrhenius plots of the chain diffusion coefficients (a) and plot illustrating the surface dependence of the activation energies (b).

3.2 Rouse mode analysis

The polymer chain dynamics can be further characterized by investigating their conformational relaxation dynamics, which is commonly characterized through the autocorrelation functions $C_p(t) = \langle Q_p(0) \cdot Q_p(t) \rangle$ of the Rouse Normal Modes (RNMs):

$$Q_p(t) = \frac{1}{N}\sum_{j=1}^{N} r_j(t)\, cos\left[\frac{\left(j-\frac{1}{2}\right)p\pi}{N}\right] \qquad (5)$$

where $r_j(t)$ is the position of monomer j at time t, and p=1, 2, ..., N-1 is the mode index. Each mode p is associated with a typical length-scale, as it describes the collective motion of chain sections containing the N/p beads. Note that the polymer center-of-mass, which is relevant to the translational diffusion described previously, formally corresponds to the mode p=0. In the following, we focus on the system with f=0.50.

Fig. 4(a) shows $C_p(t)$ for different values of p at temperature T*=1.0. Their decay becomes significantly faster with increasing p, as the mode describes more localized motions. The decay of the autocorrelation functions appear to be not consistent with a simple exponential, as predicted by the Rouse model, being , instead, well described by a stretched exponential, or Kohlrausch-Williams-Watts (KWW) function:

$$C_p(t) \simeq \exp\left[-\left(t/\tau_p^s\right)^{\beta}\right] \qquad (6)$$

This behaviour has been also reported in simulations of polymer matrix embedding polymer grafted nanoparticles[41] and is generally known to be a common hallmark of glassiness and an indirect signature of the emergence of dynamic heterogeneities.[42] It is worth noticing that a crossover from stretched ($\beta<1$) to compressed ($\beta>1$) exponential has been also observed in soft glassy materials, such as colloidal glasses[43-46], gels[47] and other amorphous solids[48], its origin being currently a very debated issue. We extract the parameters β and τ_p^s from KWW fits to the data of Fig.4a. In addition, we directly measure the relaxation time using the standard relation, $C_p(\tau_p) = 1/e$ and found a very good agreement with the estimation obtained from fits (see, for example, Fig. 5b)

Fig. 4(b) shows that β decreases slightly on lowering the temperature but much more clearly on increasing the mode index, p, indicating that the relaxation of the chains tends to broaden on the local scale. A qualitatively similar effect was

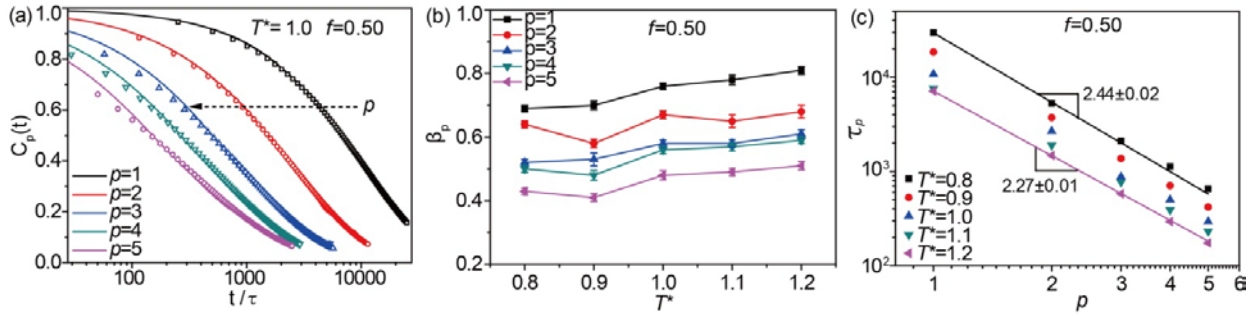

Fig. 4 (a) RNM autocorrelation function $C_p(t)$ at f=0.50, T*=1.0 and p=1, 2, . . . , 5, from right to left. The open square represents the KWW fit at different p. (b) Exponent β_p and (c) the relaxation time (τ_p, where $C_p(\tau_p)$=1/e) corresponding to the first 5 modes of polymer chains with different temperatures.

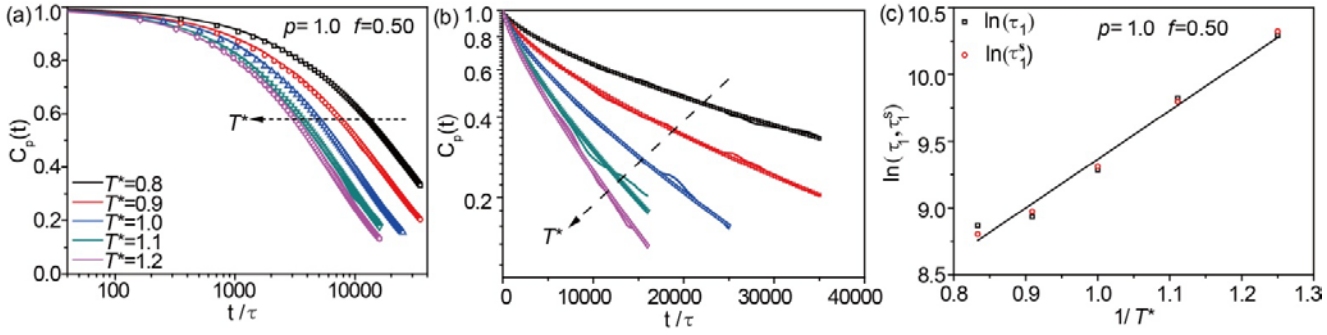

Fig. 5 (a) RNM autocorrelation function $C_p(t)$ for p=1 and T*=0.8, 0.9,..., 1.2, for heterogeneous NPs with f=0.5. The open square represents the KWW fit at different temperatures. (b) The data of panel (a) plotted in linear-log scale. (c) Fitted τ_1^s and measured τ_1 relaxation times as a function of 1/T*.

also observed in model nanocomposites with homogeneous, purely repulsive NPs by Li et al.[49]. However, at volume fractions comparable to ours, their stretching exponents for the first five modes are in the 0.7-0.9 range, i.e. much closer to unity than ours. Fig. 4(c) illustrates the dependence of the relaxation times (τ_p) on the mode index p. We point out that at high temperature, T*=1.2, the relaxation time, $\tau_p = p^{-2.27\pm0.01}$, deviates somewhat from the Rouse scaling law ($\tau_p \propto (N/p)^2$, for p<<N), and the deviation becomes even more significant at the low temperature, T*=0.8, as we find $\tau_p = p^{-2.44\pm0.02}$.

Finally, we consider the effect of the temperature on the autocorrelation functions $C_p(t)$. Fig. 5(a) shows the behavior of the mode with p=1. Decreasing temperature decreases from 1.2 to 0.8, the decay becomes slower and slower but is always properly fitted by KWW functions, allowing to measure the parameters β_p and τ_p^s as a function of T*, as shown in Fig. 4(b). Figure 5(b) clarifies that the relaxation times τ_1^s and τ_1 as a function of the temperature keeps on being consistent with an Arrhenius behaviour: $ln(\tau_1) = 3.65 \times \frac{1}{T^*} + 5.72$, the resulting activation energy being slightly larger than the one presented earlier for the translational diffusion.

In order to highlight the effect of the nanoparticle heterogeneities on the polymer chain relaxation, we compare the result of Fig. 4 and 5 to an homogeneous system with ε_{PW}=ε_{PS}=1.5ε=ε_{np}. This corresponds to a situation with chemically homogeneous nanoparticles, which have, the same average polymer-particle interactions as the system with f=0.50. The results, illustrated in Fig. 6 and 7, highlight a number of differences emerging with respect to the heterogenous case. For example, deviatons from the Rouse model appears to be weaker, especially concerning the relation between τ_p and p In addition, the stretching exponent of the KWW decreases significantly at low temperatures and increases significantly at high p, as shown in Fig. 6(d). The very good agreement between τ_1^s and τ_1 is also confirmed (Fig. 7). Finally, the activation energy is slightly lower than in the heterogeneous system: $ln(\tau_p) = 3.58 \times \frac{1}{T^*} + 5.72$. Overall, this implies that polymer relaxation is 5-10% faster than in the heterogeneous system, for the same average polymer-NP interaction strength. The difference increases on lowering the temperature.

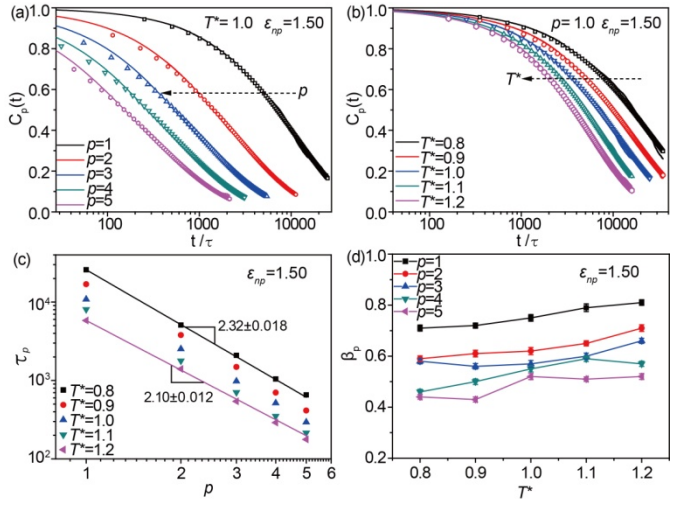

Fig. 6 For the homogeneous system with ε_{np}=1.5ε: (a) RNM autocorrelation function $C_p(t)$ at, T*=1.0 and p=1, 2, . . . , 5, from right to left. (b) RNM autocorrelation function $C_p(t)$ for p=1 and T*=0.8, 0.9, . . ., 1.2, from right to left. (c) The relaxation time (τ_p) and (d) exponent β_p for the first 5 modes of polymer chains at different temperatures.

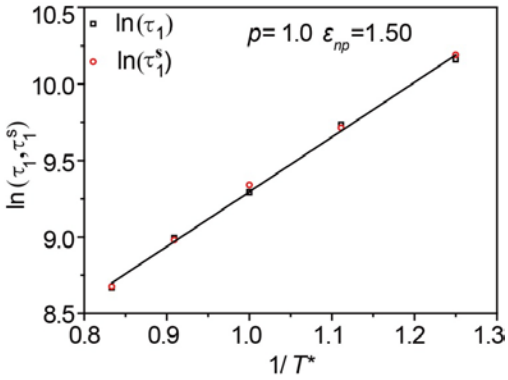

Fig. 7 Fitted τ_1^s and measured $\tau_1$relaxation time ($C_p(\tau_p)$=1/e) as a function of 1/T*. The nanocomposite filled with homogeneous nanoparticles. Note that this system have the same average polymer-particle interactions as the system with f=0.50.

3.3 Structural relaxation

In this section, we complement the previous analysis, based on the center of mass dynamics, by investigating the segmental dynamics. In particular, we compute the intermediate self scattering function (ISSF), $\phi_q^s(t)$. For an isotropic system:

$$\phi_q^s(t) = \frac{1}{M}\sum_{m=1}^{M}\langle exp(i\boldsymbol{q}\cdot[\boldsymbol{r}_m(t)-\boldsymbol{r}_m(0)])\rangle = \frac{1}{M}\sum_{m=1}^{M}\langle\frac{sin(q\Delta r_m(t))}{r_m(t)}\rangle \quad (6)$$

where M is the total number of scattering centers in the polymer matrix, $|r_m(t)-r_m(0)|=\Delta r_m(t)$ is the displacement of scattering center m after time t, and the wave-vector $q=2\pi/\lambda$, probes the dynamics at the length scale λ. Similarly to a previous work by some of us[50], we fix q=6.9 to probe the dynamics at segment length scale, i.e. the length scale relevant to the structural relaxation.

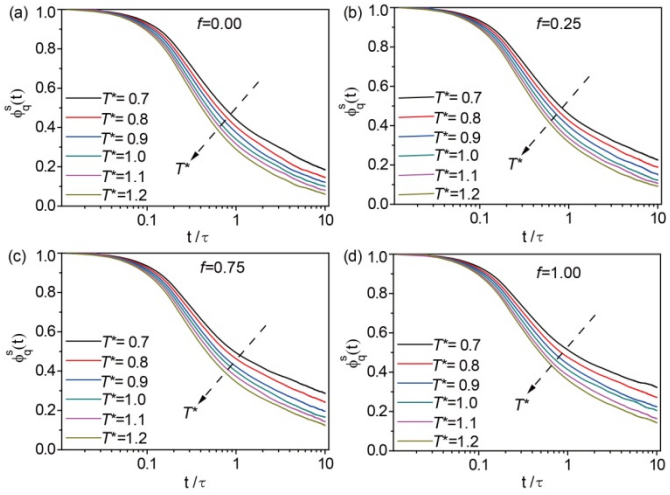

Fig. 8 ISSF, $\phi_q^s(t)$, for the system filled with heterogeneous nanoparticles at different temperatures T*=0.7, 0.8, 0.9, 1.0, 1.1 and 1.2 for different f.

Figure 10 shows the self intermediate scattering function for the heterogeneous case at different values of f. Similarly to what done for the RNM autocorrelation function, we measure the structural relaxation time, τ_{het}, from the standard relation, $\phi_q^s(\tau_{het})=e^{-1}$. Fig. 9 shows the temperature dependence τ_{het} at different value of f. Once again, data are consistent with an Arrhenius behaviour, but the activation energy monotonically increases with increasing f, differently from the diffusion constant of the chain center of mass. This difference can be rationalized considering that the segment length scale is too

small for probing the presence of disorder in the spatial distribution of W and S sites, and, therefore, the dynamics on that length is controlled by the interaction strength only.

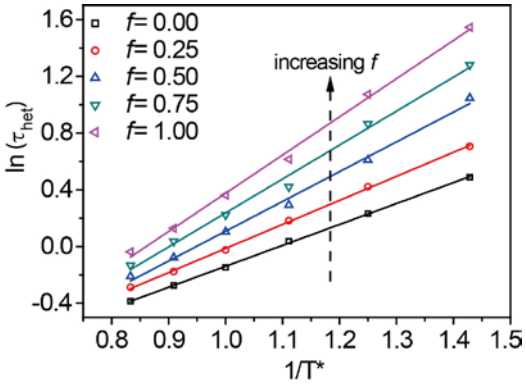

Fig. 9 Structural relaxation time as a function of $1/T^*$ for different f.

In order to further compare the effects of the heterogeneous and homogeneous nanoparticles on the polymer relaxation, Fig. 10 and Fig. 11 show $\phi_q^s(t)$ and the structural relaxation time for the heterogeneous case at f=0.5 and its homogeneous counterpart (ε_{np} =1.5), respectively. Panel b of Fig.11 clarifies that the structural relaxation time of the homogeneous system, τ_{homo} , also increases on lowering the temperature with an Arrhenius fashion. In particular, we find that $\ln(\tau_{\mathrm{het}}) = 2.10 \times \frac{1}{T^*} - 1.99$ and $\ln(\tau_{\mathrm{homo}}) = 1.92 \times \frac{1}{T^*} - 1.80$, with the associated activation energies resulting lower than those at the chain length scale. However, in both relative and absolute terms, the difference between the two activation energies increases on going from the chain length scale (+2%) for the heterogeneous nanoparticles) to the segment length scale (+9%). This is reasonable, considering that a long chain will always mediate over many energetically different situations.

Overall, it appears clearly that, in the investigated temperature range, the difference between the homogeneous and the heterogeneous case is not dramatic. However, such difference is expected to become larger and larger on decreasing the temperature. For example, at the lowest temperature investigated in this paper, T=0.7, we observe τ_{het}/τ_{homo} =1.09 that might appear a quite small difference. Conversely, at T=0.3 (a temperature that cannot be achieved in simulations but is fully accessible in experiments[29]) τ_{het}/τ_{homo} =1.5, as can be extrapolated by the Arrhenius behaviour reported in fig 8b and 9b. Accordingly, the structural relaxation time and, therefore, the zero-shear viscosity of the heterogeneous systems are expected to be 50% larger than those of the homogeneous system.

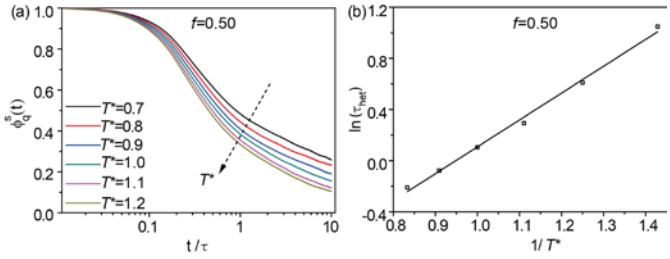

Fig. 10 (a) ISSF $\phi_q^s(t)$ for the system filled with heterogeneous nanoparticles at different temperatures T*=0.7, 0.8, 0.9, 1.0, 1.1 and 1.2. (b) Fitted relaxation times ($C_p(\tau_p)$=1/e) as a function of $1/T^*$.

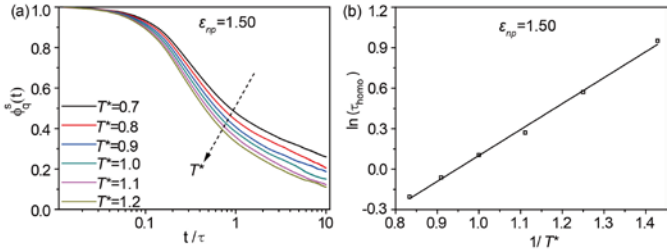

Fig. 11 (a) ISSF $\phi_q^s(t)$ for the system filled with homogeneous nanoparticles at different temperatures T*=0.7, 0.8, 0.9, 1.0, 1.1 and 1.2. (b) Structural relaxation time as a function of $1/T^*$.

IV. Conclusion

We investigated via molecular dynamics simulations a coarse-grained model of polymer filled with chemically and structurally heterogeneous nanoparticles. The heterogeneities render the model more realistic and similar to widely adopted fillers, such as carbon black. One important implication arises from the investigation of the polymer chain center of mass diffusion: the unexpected non monotonic dependence of the activation energy on the NP composition do emerge similarly to Ref. 29 and 30, although the investigated models are markedly different and reflect two different physical situations. This finding suggests the existence of a robust underlying physical

mechanism based on the interplay of interaction strength and configurational disorder. Indeed, such a non-monotonic nature disappears when focusing on the segmental dynamics, since the related probe length is too small to be sensitive to disorder.

A more general motivation of this work consists in understanding to what extent the presence of heterogeneous NPs modifies the system dynamics compared to the homogeneous case. In this respect, we clarified that relatively small differences observed at high temperature are the precursor of larger and larger changes on approaching the glass transition. This suggests that the effect of the heterogeneities may be strongly relevant for polymers forming glassy shells around nanoparticles.

Acknowledgements

This work is supported by the National Basic Research Program of China 2015CB654700(2015CB654704), the Foundation for Innovative Research Groups of the NSF of China (51221002), the National Natural Science Foundation of China (51333004 and 51403015). The cloud calculation platform of BUCT is also greatly appreciated.

References

(1) RamanathanT, A. A. Abdala, StankovichS, D. A. Dikin, M. Herrera Alonso, R. D. Piner, D. H. Adamson, H. C. Schniepp, ChenX, R. S. Ruoff, S. T. Nguyen, I. A. Aksay, R. K. Prud'Homme and L. C. Brinson, *Nat. Nano.*, 2008, **3**, 327-331.
(2) Q. Chen, S. Gong, J. Moll, D. Zhao, S. K. Kumar and R. H. Colby, *ACS Macro Lett.*, 2015, **4**, 398-402.
(3) P. Akcora, H. Liu, S. K. Kumar, J. Moll, Y. Li, B. C. Benicewicz, L. S. Schadler, D. Acehan, A. Z. Panagiotopoulos, V. Pryamitsyn, V. Ganesan, J. Ilavsky, P. Thiyagarajan, R. H. Colby and J. F. Douglas, *Nat. Mater.*, 2009, **8**, 354.
(4) J. Jancar, J. F. Douglas, F. W. Starr, S. K. Kumar, P. Cassagnau, A. J. Lesser, S. S. Sternstein and M. J. Buehler, *Polymer*, 2010, **51**, 3321-3343.
(5) A. C. Balazs, T. Emrick and T. P. Russell, *Science*, 2006, **314**, 1107.
(6) L. Wang, K. G. Neoh, E. T. Kang, B. Shuter and S.-C. Wang, *Adv. Funct. Mater.*, 2009, **19**, 2615-2622.
(7) S. Kango, S. Kalia, A. Celli, J. Njuguna, Y. Habibi and R. Kumar, *Prog. Polym. Sci.*, 2013, **38**, 1232-1261.
(8) T. Mondal, R. Ashkar, P. Butler, A. K. Bhowmick and R. Krishnamoorti, *ACS Macro Lett.*, 2016, **5**, 278-282.
(9) E. K. Lin, R. Kolb, S. K. Satija and W. l. Wu, *Macromolecules*, 1999, **32**, 3753-3757.
(10) Z. Wang, Q. Lv, S. Chen, C. Li, S. Sun and S. Hu, *ACS. Appl. Mater. Iner.*, 2016, **8**, 7499-7508.
(11) G. Maurel, F. Goujon, B. Schnell and P. Malfreyt, *J. Phys. Chem. C*, 2015, **119**, 4817-4826.
(12) D. N. Voylov, A. P. Holt, B. Doughty, V. Bocharova, H. M. Meyer, S. Cheng, H. Martin, M. Dadmun, A. Kisliuk and A. P. Sokolov, *ACS Macro Lett.*, 2017, **6**, 68-72.
(13) A. Karatrantos, R. J. Composto, K. I. Winey and N. Clarke, N., *J. Chem Phys.*, 2017, **146**, 203331.
(14) J. J. Burgos-Mármol and A. Patti, *Polymer*, 2017, **113**, 92-104.
(15) G. Tsagaropoulos and A. Eisenburg, *Macromolecules*, 1995, 28, 396-398.
(16) R. D. Priestley, C. J. Ellison, L. J. Broadbelt and J. M. Torkelson, *Science*, 2005, **309**, 456.
(17) C. J. Ellison and J. M. Torkelson, *Nat. Mater.*, 2003, **2**, 695-700.
(18) C. C. Lin, S. Gam, J. S. Meth, N. Clarke, K. I. Winey and R. J. Composto, *Macromolecules*, 2013, **46**, 4502-4509.
(19) J. T. Kalathi, S. K. Kumar, M. Rubinstein and G. S. Grest, *Soft matter*, 2015, **11**, 4123-4132.
(20) V. Ganesan and A. Jayaraman, *Soft Matter*, 2014, **10**, 13-38.
(21) J. Castillo-Tejas, S. Carro and O. Manero, *ACS Macro Lett.*, 2017, **6**, 190-193.
(22) J. Hager, R. Hentschke, N. W. Hojdis and H. A. Karimi-Varzaneh, *Macromolecules*, 2015, **48**, 9039-9049.
(23) G. D. Smith, D. Bedrov, L. Li and O. Byutner, *J. Chem Phys.*, 117, 2002 9478-9489.
(24) F. W. Starr, T. B. Schrøder and S. C. Glotzer, *Macromolecules*, 2002, **35**, 4481-4492.
(25) Y. Li, M. Kröger and W. K. Liu, *Phys. Rev. Lett.*, 2012, **109**, 118001.
(26) K. Hagita, H. Morita, M. Doi, H. Takano, *Macromolecules* 2016, **49**, 1972-1983.
(27) T. V. M. Ndoro, E. Voyiatzis, A. Ghanbari, D. N. Theodorou, M. C. Böhm and F. Müller-Plathe, *Macromolecules*, 2011, **44**, 2316-2327.
(28) A. De Nicola, R. Avolio, F. Della Monica, G. Gentile, M. Cocca, C. Capacchione, M. E. Errico and G. Milano, *RSC Adv.*, 2015, **5**, 71336-71340.
(29) G. E. Maciel and D. W. Sindorf, *J. Am. Chem. Soc.*, 1980, **102**, 7606-7607.
(30) M. L. Studebaker, E. W. D. Huffman, A. C. Wolfe and L. G. Nabors, *Ind. Eng. Chem.*, 1956, **48**, 162-166.
(31) T. A. Vilgis, *Polymer*, 2005, **46**, 4223-4229.
(32) G. D. Smith, D. Bedrov and O. Borodin, *Phys. Rev. Lett.*, 2003, **90**, 226103.
(33) A. Baumgärtner and M. Muthukumar, *M. Adv. Chem. Phys.*, 1996, 94,625-708
(34) R. Pastore and G. Raos, *Soft Matter*, 2015, **11**, 8083-8091.
(35) G. Raos and J. Idé, *ACS Macro Lett.*, 2014, **3**, 721-726.

(36) Thus, both the total and the exposed number of S beads of each NP may fluctuate according to a binomial distribution and

no spatial correlations exists among beads of the same or different type, apart from the random ones. In particular, the number of S exposed beads has mean value $<N_{es}>=N_e f$ and standard deviation, $\Delta N_{es}=[N_e f (1-f)]^{1/2}$, with a maximum value $\Delta N_{es}=4.3$ at f=0.5. While such a fluctuation is too small to affect the dynamics of this model significantly, in general it may be exploited as an additional source of heterogeneity.

(37) M. E. Mackura and D. S. Simmons, *J. Polym. Sci. Pol. Phys*. 2014, 52, 134-140.
(38) S. Plimpton, *J. Comput. Phys.* 1995, 117, 1-19.
(39) Z. Zijian, W. Zixuan, W. Lu, L. Jun, W. Youping and Z. Liqun, *Nanotechnology*, 2016, **27**, 265704.
(40) J. Liu, Y.-L. Lu, M. Tian, F. Li, J. Shen, Y. Gao and L. Zhang, *Adv. Funct. Mater.*, 2013, **23**, 1156-1163.
(41) G. D. Hattemer and G. Arya, *Macromolecule*s, 2015, **48**, 1240-1255.
(42) L. Berthier, G. Biroli, J.-P. Bouchaud, L. Cipeletti, W. van Saarloos, Dynamical Heterogeneities in Glasses, Colloids, and Granular Media, Oxford University Press, Oxford, UK, 2011.
(43) P. Ballesta, A. Duri and L. Cipelletti, *Nat. Phys*., 2008, **4**, 550–554.
(44) R. Pastore, G. Pesce and M. Caggioni, *Scientific Reports*, 2017, **7**, 43496.
(45) R. Pastore, G. Pesce, A. Sasso and M. Pica Ciamarra, *Colloid Surface A*, 2017, **532**, 87–96.
(46) R. Angelini, E. Zaccarelli, F. A. D. M. Marques, M. Sztucki, A. Fluerasu and G. Ruocco, *Nat. Commun.*, 2014, **5**, 4049.
(47) M. Bouzid, J. Colombo, L.V. Barbosa and E. Del Gado, *Nat. Commun*., 2017, **8**, 15846.
(48) E. E. Ferrero, K. Martens and J.-L. Barrat, *Phys. Rev. Lett.*, 2014, **113** ,248301.
(49) Y. Li, M. Kroger and W. K. Liu, *Soft Matter*, 2014, 10, 1723-1737.
(50) J. Liu, D. Cao, L. Zhang and W. Wang, *Macromolecules*, 2009, **42**, 2831-2842.

Please do not adjust margins